

Torsional Oscillations of Relativistic Stars with Dipole Magnetic Fields

H. Sotani^{*}, K. D. Kokkotas[†] and N. Stergioulas[‡]

Department of Physics, Aristotle University of Thessaloniki, Thessaloniki 54124, Greece

13 November 2018

ABSTRACT

We present the formalism and numerical results for torsional oscillations of relativistic stars endowed with a strong dipole magnetic field, assumed to be confined to the crust. In our approach, we focus on axisymmetric modes and neglect higher-order couplings induced by the magnetic field. We do a systematic search of parameter space by computing torsional mode frequencies for various values of the harmonic index ℓ and for various overtones, using an extended sample of models of compact stars, varying in mass, high-density equation of state and crust model. We show that torsional mode frequencies are sensitive to the crust model if the high-density equation of state is very stiff. In addition, torsional mode frequencies are drastically affected by a dipole magnetic field, if the latter has a strength exceeding roughly 10^{15} G and we find that the magnetic field effects are sensitive to the adopted crust model. Using our extended numerical results we derive empirical relations for the effect of the magnetic field on torsional modes as well as for the crust thickness. We compare our numerical results to observed frequencies in SGRs and find that certain high-density EoS and mass values are favored over others in the non-magnetized limit. On the other hand, if the magnetic field is strong, then its effect has to be taken into account in attempts to formulate a theory of asteroseismology for magnetars.

Key words: relativity – MHD – stars: neutron – stars: oscillations – stars: magnetic fields – gamma rays: theory

1 INTRODUCTION

There is growing evidence that Soft Gamma Repeaters (SGRs) could be magnetars experiencing starquakes that are connected (through the intense magnetic field) to gamma ray flare activity. Magnetars are thought to be neutron stars with very strong magnetic fields, greatly exceeding $\sim 5 \times 10^{13}$ G (Duncan & Thompson 1992). The flare activity consist of an initial short peak in the hard part of the spectrum, followed by a decaying softer part (tail) which last for hundreds of seconds. Recent analysis of detailed observations from several SGRs (Israel et al. 2005; Strohmayer & Watts 2005; Watts & Strohmayer 2006) revealed that the decaying part of the spectrum exhibits a number of oscillations with frequencies in the range of a few tenths of Hz to a few hundred Hz. There are three events detected up to now which can be associated with crust oscillations of magnetars. The first event was detected already in 1979 from the source SGR 0526-66 (Mazets et al. 1979; Barat et al. 1983), the second in 1998 from SGR 1900+14 (Hurley et al. 1999), while the third and most energetic one was observed in December 2004 from the source SGR 1802-20 (Terasawa et al. 2005; Palmer et al. 2005). Analysis of the tail oscillations of SGR 1806-20 revealed the presence of oscillations at approximately 18, 26, 29, 92.5, 150, 626.5, and 1837 Hz (Israel et al. 2005; Watts & Strohmayer 2006; Strohmayer & Watts 2006), for SGR 1900+14 the detected frequencies were 28, 54, 84, and 155 Hz (Strohmayer & Watts 2005), while for the case of SGR 0526-66 there was only one frequency identified at 43.5 Hz (Barat et al. 1983).

^{*} E-mail: sotani@astro.auth.gr

[†] E-mail: kokkotas@auth.gr

[‡] E-mail: niksterg@astro.auth.gr

Magnetar starquakes may be driven by the evolving intense magnetic field, which accumulates stress and eventually leads to crust fracturing. The excited seismic oscillations are known to be of two types: *shear modes*, which are polar-type oscillations and *torsional modes*, which are axial-type oscillations. The latter are thought to be more easily excited during a fracturing of the crust, since they only involve oscillations of the velocity, with the shear modulus of the crust acting as the necessary restoring force. Slowly rotating stars still maintain a nearly spherical shape and the velocity field of torsional oscillations is then divergence-free, with no radial component. Torsional modes (t -modes) are labeled as ℓP_n , where ℓ is the angular index, while the index n corresponds to the number of radial nodes in the eigenfunctions of the overtones for a specific ℓ . Shear and torsional modes have been studied mainly in Newtonian theory, see e.g. Hansen & Cioffi (1980); McDermott et al. (1988); Carroll et al. (1986); Strohmayer (1991); Lee (2006), while there are only a few studies of torsional modes in general relativity (Schumaker & Thorne 1983; Leins 1994; Messios et al. 2001; Samuelsson & Andersson 2006).

In the Newtonian, non-magnetized limit Hansen & Cioffi (1980) found that the period ℓP_0 of the fundamental torsional modes depends mostly on the radius of the star, R , the speed of shear waves, u_s , and the angular index ℓ , via

$$\ell P_0 \approx 2\pi[\ell(\ell+1)]^{-1/2}R/u_s, \quad (1)$$

where $u_s = (\mu/\rho)^{1/2}$, with μ and ρ being the shear modulus and the density, respectively. Furthermore, it was found that the period of overtones of index n is essentially independent of the angular index ℓ (provided ℓ does not greatly exceed n) and is basically determined by the crust thickness Δr :

$$\ell P_n \approx 2n^{-1}\Delta r/u_s. \quad (2)$$

From the above two relations it follows that the relative crust thickness, $\Delta r/R$, is given by

$$\frac{\Delta r}{R} \approx \frac{\pi n}{\sqrt{\ell(\ell+1)}} \frac{\ell f_0}{\ell f_n}, \quad (3)$$

which is independent of the details of the equation of state in the crust and basically only depends on the ratio of the frequency of the overtones to the fundamental frequency, see also Samuelsson & Andersson (2006). It thus becomes obvious that the successful identification of both the fundamental torsional frequencies and their overtones could allow for the determination of the crust thickness, which in turn could lead to information on the high-density part of the equation of state. In such a determination, of course, general relativistic and magnetic field effects on the frequencies of torsional modes should properly be taken into account, which is one of the aims of the present paper.

Relativistic effects have been found to significantly increase the fundamental $\ell = 2$ torsional mode period by roughly 30% for a typical $M = 1.4M_\odot$, $R = 10\text{km}$ model. Duncan (1998) derived the following empirical formula for the period of the fundamental $\ell = 2$ torsional mode of a relativistic star

$$\ell P_0(\text{ms}) \approx 33.6R_{10} \frac{0.87 + 0.13M_{1.4}R_{10}^{-2}}{(1.71 - 0.71M_{1.4}R_{10}^{-1})^{1/2}}, \quad (4)$$

where $R_{10} = R/(10\text{km})$ and $M_{10} = M/(1.4M_\odot)$. In this relation, two effects have been taken into account, the (relativistic) gravitational redshift and the (Newtonian) acceleration of gravity $g = GM/R^2$ at the surface. More details can be found in Duncan (1998), see also Messios et al. (2001). In addition, the formula (4) agrees well with the fully relativistic empirical relation found by Messios et al. (2001)

$$\ell P_0(\text{ms}) \approx 34R_{10}. \quad (5)$$

The latter is an extension of the Newtonian Hansen & Cioffi formula, based on a particular $1.4M_\odot$ model. On the other hand, the effect of a strong magnetic field, B , on torsional modes was considered by Duncan (1998) and Messios et al. (2001). Assuming that the shear modulus μ is augmented by the magnetic field tension, $B^2/4\pi$, one can derive the following estimate for the period of a torsional mode

$$P \approx P^{(0)} [1 + (B/B_\mu)]^{-1/2}, \quad (6)$$

where $P^{(0)}$ is the period in the limit of vanishing magnetic field and $B_\mu = \sqrt{4\pi\mu}$. However, Messios et al. (2001) found that if the structure of the magnetic field is close to monopolar in the crust, the period of the fundamental $\ell = 2$ torsional mode does not follow the above relation. This underlines the importance of properly taking into account the structure of the magnetic field, so that Equation (6) must be generalized to particular magnetic field multipoles.

An essential ingredient in computing torsional mode frequencies is the assumption one makes about the shear modulus μ . Here, we adopt the zero-temperature limit of the approximate formula derived by Strohmayer et al. (1991)

$$\mu = 0.1194 \frac{n_i(Ze)^2}{a}, \quad (7)$$

where n_i is the ion number density, $a^3 = 3/4\pi n_i$ is the average ion spacing, and $+Ze$ is the ion charge. Notice that this approximate formula for the shear modulus is derived on the assumption of a bcc crystalline state, which is averaged over

all directions. For the detailed composition of the crust, we consider a modern EOS by Douchin & Haensel (2001) (hereafter DH) and, for comparison, an older EOS by Negele & Vautherin (1973) (hereafter NV). The two EOSs for the crust differ both in composition as well as in the value of the density at the base of the crust. As the crust thickness depends on the compactness of the star, we explore the allowed parameter space for the unknown high-density EOS by selecting several tabulated high-density EOSs that yield neutron star models with significantly different macroscopic properties.

In the present work, we derive the perturbation equations for torsional oscillations of magnetized stars in general relativity following the approach by Messios et al. (2001) and neglecting spacetime perturbations (Cowling approximation). We specialize the magnetic field to a dipole structure, which allows us to reduce the system of equations to only one dimension. A large number of torsional modes (fundamental and overtones) is obtained for selected magnetar models differing in the high-density EOS, the crust EoS and mass. Our study is valid for moderate magnetic field strengths, up to roughly 10^{16} G, assuming that the magnetic field is confined to the crust and neglecting the possible presence of a thin fluid ocean. The reason for this is twofold: on one hand, for significantly stronger magnetic fields the distortion of the equilibrium shape of the star as well the magnetic coupling to higher harmonics should also be taken into account; on the other hand, the Alfvén velocity $u_A \equiv B/(4\pi\rho)^{1/2} \approx 3 \times 10^7$ cm/s $B_{15} \rho_{14}^{-1/2}$ becomes comparable to the speed of shear waves in the crust when the magnetic field reaches values of 10^{15} - 10^{16} G, which implies that global magnetosonic waves will be strongly coupled to shear waves and the torsional oscillations may no longer be confined to the crust. The effect of including global magnetosonic waves even at smaller magnetic field strengths should also be studied in more detail, see (Glampedakis et al. 2006; Sotani et al. 2006).

The article is structured as follows: in the next two sections we describe the general-relativistic ideal MHD equations, the background stellar configuration and the way that we have derived the dipole geometry of the magnetic field. In the fourth section we derive the perturbation equations for torsional oscillations of magnetized stars in the Cowling approximation, while in the fifth section we present the obtained frequencies for selected magnetar models along with fitting formulae for the influence of the magnetic field in the oscillation spectrum. The article closes with a summary and discussion.

Unless otherwise noted, we adopt units of $c = G = 1$, where c and G denote the speed of light and the gravitational constant, respectively, while the metric signature is $(-, +, +, +)$.

2 GENERAL-RELATIVISTIC IDEAL MHD

The energy momentum tensor $T^{\mu\nu}$ for a magnetized relativistic star in equilibrium, is the sum of the stress-energy tensors of a perfect fluid $T^{\mu\nu(pf)}$ and the magnetic field $T^{\mu\nu(M)}$

$$T^{\mu\nu} = T^{\mu\nu(pf)} + T^{\mu\nu(M)}, \quad (8)$$

where

$$T^{\mu\nu(pf)} = (\epsilon + p)u^\mu u^\nu + pg^{\mu\nu}, \quad (9)$$

$$T^{\mu\nu(M)} = H^2 u^\mu u^\nu + \frac{1}{2}H^2 g^{\mu\nu} - H^\mu H^\nu. \quad (10)$$

Above, ϵ , p , and H^μ are the energy density, the pressure, and a normalized magnetic field, which we define by absorbing a factor of $\sqrt{4\pi}$, i.e., $H^\mu \equiv B^\mu/\sqrt{4\pi}$, and $H^2 = H_\mu H^\mu$. Here and throughout the paper we will assume the *ideal MHD* approximation. In addition, we assume the shear modulus to be isotropic, so that there is no contribution of the shear stress in equilibrium.

Using the stress-energy tensor (8), one obtains the equations of motion of the fluid by projecting the conservation of the energy-momentum tensor on to the hypersurface normal to u^μ , i.e.,

$$h^\mu_\alpha T^{\alpha\nu}_{;\nu} = 0, \quad (11)$$

where $h^\mu_\nu = g^\mu_\nu + u^\mu u_\nu$ is the projection tensor. The equations of motion are

$$(\epsilon + p + H^2)u^\mu_{;\nu} u^\nu = -h^{\mu\nu} \left(p + \frac{1}{2}H^2 \right)_{;\nu} + h^\mu_\alpha (H^\alpha H^\nu)_{;\nu}. \quad (12)$$

Due to the ideal MHD approximation the electric field 4-vector vanishes, $E_\mu = F_{\mu\nu} u^\nu = 0$ so that the electric field is zero for a comoving observer. In this approximation, the Maxwell's equations $F_{[\mu\nu;\gamma]} = 0$, where $F_{\mu\nu}$ is the Faraday tensor, can be written in the simple form:

$$(u^\mu H^\nu - u^\nu H^\mu)_{;\mu} = 0. \quad (13)$$

In deriving the above equation the following definitions are used

$$F_{\mu\nu} = u_\mu E_\nu - u_\nu E_\mu - \epsilon_{\mu\nu\alpha\beta} u^\alpha B^\beta, \quad (14)$$

$$B_\mu = \frac{1}{2}\epsilon_{\mu\nu\alpha\beta} u^\nu F^{\alpha\beta}, \quad (15)$$

From Equation (13) one derives the magnetic induction equation

$$H^\mu_{;\nu} u^\nu = -u^\alpha_{;\alpha} H^\mu + u^\mu_{;\nu} H^\nu + H^\alpha u_{\alpha;\beta} u^\beta u^\mu, \quad (16)$$

$$= \left(\sigma^\mu_\nu + \omega^\mu_\nu - \frac{2}{3} \delta^\mu_\nu \Theta \right) H^\nu + H^\alpha u_{\alpha;\beta} u^\beta u^\mu, \quad (17)$$

where $\sigma_{\mu\nu}$ is the rate of shear tensor, $\omega_{\mu\nu}$ is the twist tensor and Θ is the expansion, defined as

$$\Theta \equiv u^\mu_{;\mu}, \quad (18)$$

$$\sigma_{\mu\nu} \equiv \frac{1}{2} (u_{\mu;\alpha} h^\alpha_\nu + u_{\nu;\alpha} h^\alpha_\mu) - \frac{1}{3} \Theta h_{\mu\nu}, \quad (19)$$

$$\omega_{\mu\nu} \equiv \frac{1}{2} (u_{\mu;\alpha} h^\alpha_\nu - u_{\nu;\alpha} h^\alpha_\mu). \quad (20)$$

In a following section, the above equations will be linearized, in order to obtain the perturbed equations of motion describing small-amplitude oscillations. But first, we describe the construction of the background equilibrium models.

3 EQUILIBRIUM CONFIGURATION

A strongly magnetized relativistic star has a non-spherical shape, due to the tension of the magnetic field, which is expressed via the off-diagonal components in the stress-energy tensor $T^{\mu\nu}$. However, the deformations from spherical symmetry induced by the magnetic field are small for neutron stars with magnetic field usually assumed for magnetars, because the energy of the magnetic field is considerably smaller than the gravitational energy, i.e.,

$$\frac{\text{magnetic energy}}{\text{gravitational energy}} \sim \frac{B^2 R^3}{GM^2/R} \sim 10^{-4} \left(\frac{B}{10^{16}[\text{G}]} \right)^2. \quad (21)$$

For this reason, we neglect the deformations due to magnetic fields in the construction of equilibrium models. Since magnetars are also extremely slowly rotating (the intense magnetic field spins down the star on a short timescale) we can also neglect any rotational deformations, so that the equilibrium models can be considered as spherically symmetric solutions of the well-known TOV equations described by a metric of the form

$$ds^2 = -e^{2\Phi} dt^2 + e^{2\Lambda} dr^2 + r^2 (d\theta^2 + \sin^2 \theta d\phi^2), \quad (22)$$

where Φ and Λ are the function of the Schwarzschild radial coordinate r . The four-velocity of the equilibrium model is thus $u^\mu = (e^{-\Phi}, 0, 0, 0)$. (23)

We supplement the equilibrium model by a dipole magnetic field (but see Braithwaite & Spruit (2006) for other assumptions), following the approach of Konno et al. (1999) i.e. we consider an axisymmetric, poloidal magnetic field, which is created by a 4-current $J_\mu = (0, 0, 0, J_\phi)$. In ideal MHD the electromagnetic 4-potential A_μ is very simple and has only one component in spherical polar coordinates

$$A_\mu = (0, 0, 0, A_\phi), \quad (24)$$

with

$$F_{\mu\nu} = A_{\nu,\mu} - A_{\mu,\nu}, \quad (25)$$

(Bocquet et al. 1995; Konno et al. 1999). For the metric chosen above, Maxwell's equations $F^{\mu\nu}_{;\nu} = 4\pi J^\mu$ lead to the following elliptic equation for A_ϕ

$$e^{-2\Lambda} \frac{\partial^2 A_\phi}{\partial r^2} + \frac{1}{r^2} \frac{\partial^2 A_\phi}{\partial \theta^2} + (\Phi' - \Lambda') e^{-2\Lambda} \frac{\partial A_\phi}{\partial r} - \frac{1}{r^2} \frac{\cos \theta}{\sin \theta} \frac{\partial A_\phi}{\partial \theta} = -4\pi J_\phi. \quad (26)$$

The 4-vectors A_μ and J_μ can be expanded in vector spherical harmonics, so that

$$A_\phi(r, \theta) = a_{\ell_M}(r) \sin \theta \partial_\theta P_{\ell_M}(\cos \theta), \quad (27)$$

$$J_\phi(r, \theta) = j_{\ell_M}(r) \sin \theta \partial_\theta P_{\ell_M}(\cos \theta), \quad (28)$$

where $a_{\ell_M}(r)$ and $j_{\ell_M}(r)$ are functions of the radial coordinate only. This leads to a one-dimensional form of Equation (26)

$$e^{-2\Lambda} \frac{d^2 a_{\ell_M}}{dr^2} + (\Phi' - \Lambda') e^{-2\Lambda} \frac{da_{\ell_M}}{dr} - \frac{\ell_M(\ell_M + 1)}{r^2} a_{\ell_M} = -4\pi j_{\ell_M}. \quad (29)$$

For a dipole magnetic field, i.e., $\ell_M = 1$, an analytic exterior solution for a_1 exists, setting $j_1^{(\text{ex})} = 0$ and $e^{2\Phi} = e^{-2\Lambda} = 1 - 2M/r$ (Wasserman & Shapiro 1983)

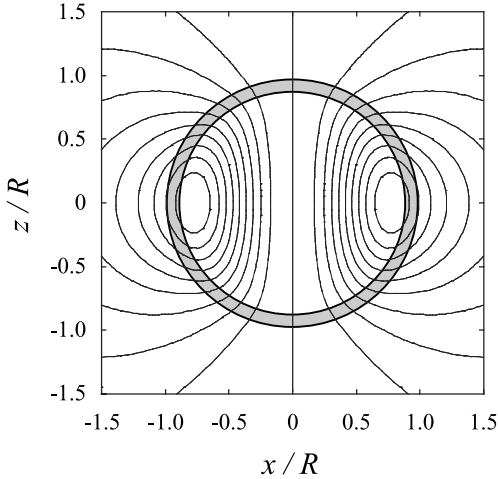


Figure 1. Magnetic field lines of a typical equilibrium model. At the surface, an analytic solution for an exterior dipole magnetic field is smoothly joined to a numerical interior solution. The grey area shows the crust region, to which the magnetic field is assumed to be effectively confined when computing the torsional oscillations.

$$a_1^{(\text{ex})} = -\frac{3\mu_b}{8M^3}r^2 \left[\ln\left(1 - \frac{2M}{r}\right) + \frac{2M}{r} + \frac{2M^2}{r^2} \right], \quad (30)$$

where μ_b is the magnetic dipole moment for an observer at infinity. In the interior the potential $a_1^{(\text{in})}$ is found by solving numerically Equation (29). The current distribution $j_1^{(\text{in})}$, which is the source term of Equation (29) must satisfy the integrability condition that the solution is stationary (Bonazzola et al. 1993). Here we adopt the same, simplified form for the current distribution as the one used in Konno et al. (1999), i.e.,

$$j_1^{(\text{in})} = f_0 r^2 (\epsilon + p), \quad (31)$$

where f_0 is an arbitrary constant. Moreover, regularity at the center of the star implies that $a_1^{(\text{in})}$ has the form

$$a_1^{(\text{in})} = \alpha_c r^2 + \mathcal{O}(r^4), \quad (32)$$

where α_c is a constant, which is determined by the junction condition with $a_1^{(\text{ex})}$ at stellar surface. Finally, the components of the vector H_μ describing the normalized magnetic field are given by the following set of equations

$$H_r = -\frac{e^\Lambda}{\sqrt{4\pi r^2 \sin \theta}} \partial_\theta A_\phi = \frac{e^\Lambda \cos \theta}{\sqrt{\pi r^2}} a_1, \quad (33)$$

$$H_\theta = \frac{e^{-\Lambda}}{\sqrt{4\pi \sin \theta}} \partial_r A_\phi = -\frac{e^{-\Lambda} \sin \theta}{\sqrt{4\pi}} a_{1,r}. \quad (34)$$

Figure 1 shows the magnetic field lines of the complete solution, for a typical equilibrium configuration. We emphasize that, even though the magnetic field configuration has been computed throughout the star, the boundary conditions we will assume for the torsional oscillations will neglect the presence of the magnetic field outside the crust region, so that, effectively, that magnetic field will be assumed to be confined to the crust only.

4 PERTURBATION EQUATIONS

4.1 Covariant form

The perturbation equations are derived by linearizing the equations of motion (12) and the magnetic induction equation (16). Since we only consider torsional oscillations, which are of axial type and do not induce density variations in spherical stars, there is no significant variation in the radiative part of the metric describing the gravitational field. In addition, since torsional modes are essentially material velocity oscillations, the imaginary part of their frequency due to the emission of current-multipole gravitational radiation is much smaller than the real part. For these reasons the frequency of torsional oscillations is determined with satisfactory accuracy even when neglecting entirely the metric perturbations by setting $\delta g_{\mu\nu} = 0$ (i.e. adopting the relativistic Cowling approximation), see Leins (1994) and we adopt this approximation here.

The linearized form of the equation of motion (12) is

$$(\epsilon + p + H^2) \delta u^\mu_{;\nu} u^\nu = -(\delta \epsilon + \delta p + 2H_\alpha \delta H^\alpha) u^\mu_{;\nu} u^\nu - (\epsilon + p + H^2) u^\mu_{;\nu} \delta u^\nu$$

$$\begin{aligned}
& + (u^\mu \delta u_\alpha + \delta u^\mu u_\alpha) \left[H^\alpha H^\nu - g^{\alpha\nu} \left(p + \frac{1}{2} H^2 \right) \right]_{;\nu} \\
& + h^\mu_\alpha \left[H^\alpha \delta H^\nu + \delta H^\alpha H^\nu - g^{\alpha\nu} (\delta p + H_\beta \delta H^\beta) \right]_{;\nu} - h^\mu_\alpha \delta T^{\alpha\nu(s)}_{;\nu}.
\end{aligned} \tag{35}$$

where $\delta T^{\mu\nu(s)}$ is the linearized shear stress tensor. The latter is assumed to be related to the linearized shear tensor $\delta S_{\mu\nu}$, through

$$\delta T_{\mu\nu}^{(s)} = -2\mu \delta S_{\mu\nu}, \tag{36}$$

see Schumaker & Thorne (1983). In addition, linearization of the magnetic induction equation (16) yields

$$\begin{aligned}
\delta H^\mu_{;\nu} u^\nu & = -H^\mu_{;\nu} \delta u^\nu + h^{\mu\alpha} \delta u_{\alpha;\beta} H^\beta + h^{\mu\alpha} u_{\alpha;\beta} \delta H^\beta + u^\mu \delta u^\alpha H^\beta u_{\alpha;\beta} - \delta \Theta H^\mu - \Theta \delta H^\mu \\
& + u^\mu H^\alpha (\delta u_{\alpha;\beta} u^\beta + u_{\alpha;\beta} \delta u^\beta) + (H^\alpha \delta u^\mu + \delta H^\alpha u^\mu) u_{\alpha;\beta} u^\beta,
\end{aligned} \tag{37}$$

where we used $u^\alpha \delta u_{\alpha;\beta} = -\delta u^\alpha u_{\alpha;\beta}$. Notice that the above relation differs in some terms from Equation (12) in Messios et al. (2001), due to a sign error in the latter reference¹. In Appendix A we also give the corrected equations and numerical results for the special magnetic field configuration considered in Messios et al. (2001).

4.2 Axial Perturbations

The usual method for studying matter perturbations of spherically symmetric backgrounds is to decompose the perturbed quantities into scalar and vector spherical harmonics of definite indices ℓ and m . In this way, the different oscillation modes characterized by ℓ and m decouple and one can study them independently. Here we restrict attention to axial-type perturbations, for which the perturbed matter quantities can be written as

$$\delta\epsilon = \delta p = 0, \tag{38}$$

$$\delta u^t = \delta u^r = \delta u^\theta = 0, \tag{39}$$

$$\delta u^\phi = e^{-\Phi} \partial_t \mathcal{Y}(t, r) b(\theta), \tag{40}$$

where

$$b(\theta) \equiv \frac{1}{\sin \theta} \partial_\theta P_\ell(\cos \theta), \tag{41}$$

where ∂_θ denotes the partial derivative with respect to θ . Above, $\mathcal{Y}(t, r)$ describes the radial dependence of the angular displacement of the stellar material, $P_\ell(\cos \theta)$ is the Legendre polynomial of order ℓ and we have set $m = 0$, due to the degeneracy in m for spherically symmetric backgrounds. The above assumptions lead to the following form of the ϕ -component of the linearized equation of motion (35)

$$\begin{aligned}
(\epsilon + p + H^2) e^{-\Phi} \delta u_{,t}^\phi & = \delta H^r \left[H_{,r}^\phi + H^\phi \left(\Phi_{,r} + \Lambda_{,r} + \frac{4}{r} \right) - \frac{e^{2\Lambda} H_{,r}^\phi}{r^2 \sin^2 \theta} \right] + \delta H^\theta \left[H_{,\theta}^\phi + 3 \cot \theta H^\phi - \frac{H_{,\theta}^\phi}{\sin^2 \theta} \right] \\
& + \delta H^\phi \left[2 \cot \theta H^\theta + \left(\Phi_{,r} + \frac{2}{r} \right) H^r \right] + H^\phi (\delta H^t_{,t} + \delta H^r_{,r} + \delta H^\theta_{,\theta} + \delta H^\phi_{,\phi}) + H^r \delta H^\phi_{,r} + H^\theta \delta H^\phi_{,\theta} \\
& - \frac{H^r \delta H_{r,\phi}}{r^2 \sin^2 \theta} - \frac{H^\theta \delta H_{\theta,\phi}}{r^2 \sin^2 \theta} - \delta T^r_{,r}^{\phi(s)} - \delta T^\theta_{,\theta}^{\phi(s)} - \left(\frac{4}{r} + \Phi_{,r} + \Lambda_{,r} \right) \delta T^r \phi(s) - 3 \cot \theta \delta T^\theta \phi(s),
\end{aligned} \tag{42}$$

where we used the relation $H_{;\alpha}^\alpha = u_{;\beta}^\alpha u^\beta H_\alpha$, which is derived from the Maxwell's equations.

For the derivation of the linearized shear tensor $\delta S_{\mu\nu}$, we adopt the relationship $\delta \sigma_{\mu\nu} = \mathcal{L}_u \delta S_{\mu\nu}$ (Carter & Quintana 1972; Schumaker & Thorne 1983), which becomes

$$\delta \sigma_{\mu\nu} = e^{-\Phi} \delta S_{\mu\nu,t} \tag{43}$$

In the Cowling approximation the only nonvanishing components of $\delta \sigma_{\mu\nu}$ are written as

$$\delta \sigma_{r\phi} = \frac{1}{2} r^2 e^{-\Phi} \mathcal{Y}_{,tr} b \sin^2 \theta \quad \text{and} \quad \delta \sigma_{\theta\phi} = \frac{1}{2} r^2 e^{-\Phi} \mathcal{Y}_{,t\theta} b \sin^2 \theta, \tag{44}$$

It follows that the only non-vanishing components of the linearized shear stress tensor are

$$\delta T_{r\phi}^{(s)} = -\mu r^2 \mathcal{Y}_{,r} b \sin^2 \theta, \tag{45}$$

$$\delta T_{\theta\phi}^{(s)} = -\mu r^2 \mathcal{Y}_{,\theta} b \sin^2 \theta. \tag{46}$$

¹ A sign error adopted initially from another publication propagated throughout the magnetic terms in the equations and final numerical results presented in that paper. We have confirmed that all equations and results in the non-magnetized limit were correct, while also the qualitative behaviour of the fundamental torsional mode as a function of the magnetic field strength was correct (see Appendix A).

The linearized induction equation (37) yields that following relations for the first time-derivative of the components of δH^μ

$$\delta H_{,t}^t = e^{-\Phi} H^\phi \delta u_{\phi,t}, \quad (47)$$

$$\delta H_{,t}^r = -e^\Phi H_{,\phi}^r \delta u^\phi, \quad (48)$$

$$\delta H_{,t}^\theta = -e^\Phi H_{,\phi}^\theta \delta u^\phi, \quad (49)$$

$$\delta H_{,t}^\phi = e^\Phi [(\Phi_{,r} H^r - H_{,\phi}^\phi) \delta u^\phi + H^r \delta u_{,r}^\phi + H^\theta \delta u_{,\theta}^\phi]. \quad (50)$$

Substituting the previous relations into the linearized equations of motion (42) and assuming that all perturbed variables have a harmonic time dependence, such that $\mathcal{Y}(t, r) = e^{i\omega t} \mathcal{Y}(r)$, one obtains

$$\begin{aligned} -[\epsilon + p + H^2 - (H^\phi r \sin \theta)^2] \omega^2 e^{-2\Phi} \mathcal{Y} &= e^{-2\Lambda} \mu \mathcal{Y}'' + \left[\left(\frac{4}{r} + \Phi' - \Lambda' \right) \mu + \mu' \right] e^{-2\Lambda} \mathcal{Y}' - \frac{(\ell + 2)(\ell - 1)}{r^2} \mu \mathcal{Y} \\ &- \left\{ H_{,\phi}^r H_{,r}^\phi + H_{,\phi}^r H^\phi \left(\Phi' + \Lambda' + \frac{4}{r} \right) + H_{,\phi}^\theta H_{,\theta}^\phi + 3 \cot \theta H_{,\phi}^\theta H^\phi \right. \\ &- \frac{1}{r^2 \sin^2 \theta} e^{2\Lambda} [(H_{,\phi}^r)^2 + H^r H_{,\phi\phi}^r] - \frac{1}{\sin^2 \theta} [(H_{,\phi}^\theta)^2 + H^\theta H_{,\phi\phi}^\theta] \\ &+ H_{,\phi}^\phi \left[2 \cot \theta H^\theta + \left(\Phi' + \frac{2}{r} \right) H^r \right] + H^\phi (H_{,r\phi}^r + H_{,\theta\phi}^\theta + H_{,\phi\phi}^\phi) + H^r H_{,r\phi}^\phi \\ &+ H^\theta H_{,\theta\phi}^\phi \left\} \mathcal{Y} + \left[2 \cot \theta H^r H^\theta + \left(\Phi' + \frac{2}{r} \right) (H^r)^2 + H^r (H_{,r}^r - H_{,\phi}^\phi) + H^\theta H_{,r\theta}^\theta \right] \mathcal{Y}' \\ &+ (H^r)^2 \mathcal{Y}'' + \left\{ \left[\left(\Phi' + \frac{2}{r} \right) H^r H^\theta + H^r H_{,r}^\theta + 2 \cot \theta (H^\theta)^2 + H^\theta (H_{,\theta}^\theta - H_{,\phi}^\phi) \right] \mathcal{Y} \right. \\ &+ 2 H^r H^\theta \mathcal{Y}' \left. \right\} \frac{b_{,\theta}}{b} + (H^\theta)^2 \mathcal{Y} \frac{b_{,\theta\theta}}{b}, \end{aligned} \quad (51)$$

where a prime (') denotes the derivative with respect to r . The above eigenvalue equation for the mode-frequency ω is still written for a general equilibrium magnetic field $H^\mu(r, \theta, \phi)$.

4.3 Dipole magnetic field

Restricting attention to an axisymmetric poloidal magnetic field, the eigenvalue equation (51) becomes

$$\begin{aligned} -[\epsilon + p + H^r H_r + H^\theta H_\theta] \omega^2 e^{-2\Phi} \mathcal{Y} &= e^{-2\Lambda} \mu \mathcal{Y}'' + \left[\left(\frac{4}{r} + \Phi' - \Lambda' \right) \mu + \mu' \right] e^{-2\Lambda} \mathcal{Y}' - (\ell + 2)(\ell - 1) \left[\frac{\mu}{r^2} + (H^\theta)^2 \right] \mathcal{Y} \\ &+ \left[2 \cot \theta H^r H^\theta + \left(\Phi' + \frac{2}{r} \right) (H^r)^2 + H^r H_{,r}^r + H^\theta H_{,\theta}^r \right] \mathcal{Y}' + (H^r)^2 \mathcal{Y}'' \\ &+ \left\{ \left[\left(\Phi' + \frac{2}{r} \right) H^r H^\theta + H^r H_{,r}^\theta - \cot \theta (H^\theta)^2 + H^\theta H_{,\theta}^\theta \right] \mathcal{Y} + 2 H^r H^\theta \mathcal{Y}' \right\} \frac{b_{,\theta}}{b}, \end{aligned} \quad (52)$$

where we used the following equation satisfied by the angular function $b(\theta)$

$$b_{,\theta\theta} + 3 \cot \theta b_{,\theta} + (\ell + 2)(\ell - 1)b = 0. \quad (53)$$

The above eigenvalue equation can be simplified further by assuming a dipole magnetic field of the form (33), (34). We achieve this by first writing Equation (52) in the form

$$[\mathcal{A}_\ell(r) + \mathcal{B}_\ell(r)] \partial_\theta Y_{\ell 0} + [\mathcal{C}_\ell(r) - \mathcal{B}_\ell(r)] \sin^2 \theta \partial_\theta Y_{\ell 0} + \mathcal{D}_\ell(r) \sin \theta \cos \theta Y_{\ell 0} = 0, \quad (54)$$

where $Y_{\ell 0}$ is the spherical harmonic function with $m = 0$, which is related to $P_\ell(\cos \theta)$ via the normalization $Y_{\ell 0} = \sqrt{(2\ell + 1)/(4\pi)} P_\ell$. The four radial functions $\mathcal{A}_\ell(r)$, $\mathcal{B}_\ell(r)$, $\mathcal{C}_\ell(r)$, and $\mathcal{D}_\ell(r)$ are

$$\mathcal{A}_\ell(r) = \mu \mathcal{Y}'' + \left[\left(\frac{4}{r} + \Phi' - \Lambda' \right) \mu + \mu' \right] \mathcal{Y}' + \left[(\epsilon + p) \omega^2 e^{-2\Phi} - \frac{(\ell + 2)(\ell - 1)}{r^2} \mu \right] e^{2\Lambda} \mathcal{Y}, \quad (55)$$

$$\mathcal{B}_\ell(r) = \frac{a_1}{\pi r^4} \{ a_1 \mathcal{Y}'' + [(\Phi' - \Lambda') a_1 + 2a_1'] \mathcal{Y}' + [\omega^2 e^{-2\Phi+2\Lambda} a_1 + (\Phi' - \Lambda') a_1' + a_1''] \mathcal{Y} \}, \quad (56)$$

$$\mathcal{C}_\ell(r) = \frac{a_1'}{4\pi r^4} \{ 2a_1 \mathcal{Y}' + [\omega^2 e^{-2\Phi} r^2 - (\ell + 2)(\ell - 1)] a_1' \mathcal{Y} \}, \quad (57)$$

$$\mathcal{D}_\ell(r) = \frac{\ell(\ell + 1)}{2\pi r^4} a_1 \{ 2a_1' \mathcal{Y}' + [(\Phi' - \Lambda') a_1' + a_1''] \mathcal{Y} \}, \quad (58)$$

in which the magnetic field now appears through the radial function a_1 of Equations (33) and (34).

Multiplying Equation (54) with $\partial_\theta Y_{\ell 0}^*$ and integrating over the sphere, the eigenvalue equations takes the 1-dimensional form

$$\ell(\ell+1)(\mathcal{A}_\ell + \mathcal{B}_\ell) + \mathcal{L}_1^{\pm 2}(\mathcal{C}_\ell - \mathcal{B}_\ell) + \mathcal{L}_2^{\pm 2}\mathcal{D}_\ell = 0. \quad (59)$$

In deriving this equation we used the following properties of spherical harmonic functions:

$$\ell(\ell+1)\mathcal{A}_\ell := \sum_{\ell'} \mathcal{A}_{\ell'} \int (\partial_\theta Y_{\ell 0}^*) (\partial_\theta Y_{\ell' 0}) d\Omega, \quad (60)$$

$$\begin{aligned} \mathcal{L}_1^{\pm 2}\mathcal{A}_\ell &:= \sum_{\ell'} \mathcal{A}_{\ell'} \int (\partial_\theta Y_{\ell 0}^*) \sin^2 \theta (\partial_\theta Y_{\ell' 0}) d\Omega \\ &= -\ell(\ell+3)Q_{\ell+2}Q_{\ell+1}\mathcal{A}_{\ell+2} + [\ell^2 Q_{\ell+1}^2 + (\ell+1)^2 Q_\ell^2] \mathcal{A}_\ell - (\ell-2)(\ell+1)Q_\ell Q_{\ell-1}\mathcal{A}_{\ell-2}, \end{aligned} \quad (61)$$

$$\begin{aligned} \mathcal{L}_2^{\pm 2}\mathcal{A}_\ell &:= \sum_{\ell'} \mathcal{A}_{\ell'} \int (\partial_\theta Y_{\ell 0}^*) \sin \theta \cos \theta Y_{\ell' 0} d\Omega \\ &= \ell Q_{\ell+1}Q_{\ell+2}\mathcal{A}_{\ell+2} + [\ell Q_{\ell+1}^2 - (\ell+1)Q_\ell^2] \mathcal{A}_\ell - (\ell+1)Q_\ell Q_{\ell-1}\mathcal{A}_{\ell-2}, \end{aligned} \quad (62)$$

$$Q_\ell := \sqrt{\frac{\ell^2}{(2\ell-1)(2\ell+1)}}. \quad (63)$$

From Equations (59), (61) and (62) it is evident that the presence of the dipole magnetic field causes the eigenfunction of a specific torsional $(\ell, 0)$ mode to be no longer described by an angular part that corresponds to a single value of ℓ (as in the nonmagnetized case). Instead, the eigenfunction of a specific mode also acquires pieces with $\ell+2$, $\ell-2$ and higher order dependence (through successive couplings). In order to solve the full problem to a desired accuracy, one has to solve a linear system of equations of the type (59) for required values of ℓ , up to some finite ℓ_{\max} . Since the coupling is purely a magnetic field effect, in the absence of a magnetic field the radial functions \mathcal{B}_ℓ , \mathcal{C}_ℓ , and \mathcal{D}_ℓ vanish and the different ℓ dependencies decouple.

4.4 Neglecting $\ell \pm 2$ couplings

As mentioned in the introduction, we limit our current study to moderate magnetic field strengths of a few times 10^{15} G, since for larger values one would also have to take into account global magnetosonic oscillations. We further simplify the numerical problem, by neglecting the couplings to $\ell \pm 2$ terms in Equation (59). This is motivated by the expectation that higher-order contributions will be less significant than the lowest-order piece of an eigenfunction, since the higher-order pieces are sampling the background magnetic field at smaller scales. This expectation may be valid for the study of low-order modes. However, it is difficult to predict the effect of $\ell \pm 2$ couplings on high-order modes without solving the full two-dimensional problem. Our numerical results will thus be valid only to the extend that magnetic-field-induced couplings to $\ell \pm 2$ terms can be neglected.

Neglecting $\ell \pm 2$ couplings leads to the eigenvalue equation

$$\begin{aligned} \left[\mu + (1+2\lambda_1) \frac{a_1^2}{\pi r^4} \right] \mathcal{Y}'' &+ \left\{ \left(\frac{4}{r} + \Phi' - \Lambda' \right) \mu + \mu' + (1+2\lambda_1) \frac{a_1}{\pi r^4} [(\Phi' - \Lambda') a_1 + 2a_1'] \right\} \mathcal{Y}' \\ &+ \left\{ \left[\left(\epsilon + p + (1+2\lambda_1) \frac{a_1^2}{\pi r^4} \right) e^{2\Lambda} - \frac{\lambda_1 a_1'^2}{2\pi r^2} \right] \omega^2 e^{-2\Phi} \right. \\ &\quad \left. - (\lambda - 2) \left(\frac{\mu e^{2\Lambda}}{r^2} - \frac{\lambda_1 a_1'^2}{2\pi r^4} \right) + (2+5\lambda_1) \frac{a_1}{2\pi r^4} \{(\Phi' - \Lambda') a_1' + a_1''\} \right\} \mathcal{Y} = 0, \end{aligned} \quad (64)$$

where

$$\lambda = \ell(\ell+1), \quad (65)$$

$$\lambda_1 = \ell Q_{\ell+1}^2 - (\ell+1)Q_\ell^2 = -\frac{\ell(\ell+1)}{(2\ell-1)(2\ell+3)}. \quad (66)$$

In order to solve a system of first-order ODEs, we define new variables \mathcal{Y}_1 and \mathcal{Y}_2 , through

$$\mathcal{Y}_1 \equiv \mathcal{Y} r^{1-\ell}, \quad (67)$$

$$\mathcal{Y}_2 \equiv \left[\mu + (1+2\lambda_1) \frac{a_1^2}{\pi r^4} \right] e^{\Phi-\Lambda} \mathcal{Y}' r^{2-\ell}. \quad (68)$$

In defining the new variables, we took into account the form of the eigenfunction \mathcal{Y} near the center, where $\mathcal{Y} \sim r^{\ell-1}$. The

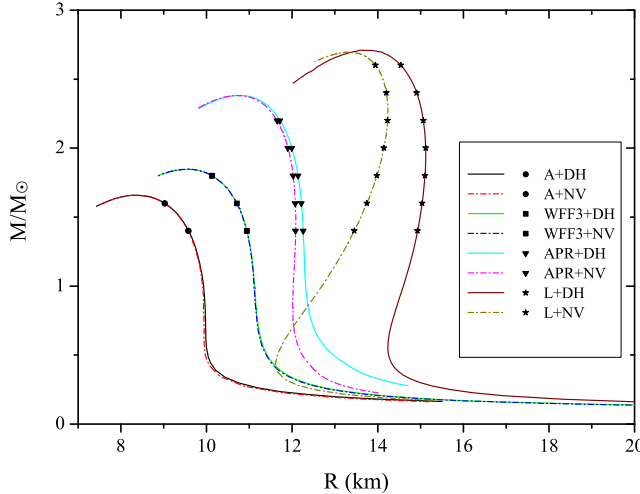


Figure 2. Mass-radius relationship of nonrotating equilibrium models constructed with various high-density EoS, in combination with the two choices for the crust EoS. Individual models for which we compute torsional modes are shown with symbols.

final first-order system of equations to be solved numerically for the real eigenvalues ω is then

$$\mathcal{Y}_1' = -\frac{\ell-1}{r}\mathcal{Y}_1 + \frac{\pi r^3}{\pi r^4 \mu + (1+2\lambda_1)a_1^2} e^{-\Phi+\Lambda} \mathcal{Y}_2, \quad (69)$$

$$\begin{aligned} \mathcal{Y}_2' = & -\left[\left(\epsilon + p + (1+2\lambda_1) \frac{a_1^2}{\pi r^4} - \lambda_1 e^{-2\Lambda} \frac{a_1'^2}{2\pi r^2} \right) \omega^2 r e^{2(\Lambda-\Phi)} \right. \\ & \left. - (\lambda-2) \left(\frac{\mu e^{2\Lambda}}{r} - \frac{\lambda_1 a_1'^2}{2\pi r^3} \right) + (2+5\lambda_1) \frac{a_1 e^{2\Lambda}}{\pi r^3} \left(\frac{a_1}{r^2} - 2\pi j_1 \right) \right] e^{\Phi-\Lambda} \mathcal{Y}_1 - \frac{\ell+2}{r} \mathcal{Y}_2, \end{aligned} \quad (70)$$

where Equation (29) was used in order to eliminate the term of a_1'' .

4.5 Boundary conditions

If one would solve the above system of equations from the center of the star to the surface, then regularity at the center implies the boundary condition

$$\mathcal{Y}_2 = (\ell-1) \left[\mu + (1+2\lambda_1) \frac{\alpha_c^2}{\pi} \right] e^{\Phi} \mathcal{Y}_1. \quad (71)$$

If the equations (69)-(70) are used for the study of global oscillations, i.e. magnetosonic waves in the core and the crust and shear waves in the crust, an appropriate boundary condition at the base of the fluid/crust interface will be $\mathcal{Y}_2^{(-)} = \mathcal{Y}_2^{(+)}$ which leads to the condition

$$\mathcal{Y}'^{(-)} = \left[1 + \frac{1}{1+2\lambda_1} \frac{u_s^2}{u_A^2} \right] \mathcal{Y}'^{(+)}. \quad (72)$$

This is analogous to the one used by Glampedakis et al. (2006) in their study of a corresponding toy problem.

However, here, we only consider torsional modes confined to the crust and impose a zero traction condition at the base of the crust, which implies that $\mathcal{Y}_2 = 0$ there. At the stellar surface, the “zero-torque-at-surface” condition is imposed, i.e. $\delta T_{\phi}^{(s)r} = 0$ (Schumaker & Thorne 1983), which again implies $\mathcal{Y}_2 = 0$ with our choice of variables. We neglect the possible presence of a thin fluid ocean.

Table 1. Mass (M), Radius (R) and relative crust thickness ($\Delta r/R$) for specific equilibrium models constructed with various high-density EoS (A, WFF3, APR and L) in combination with two crust EoS (DH and NV). The subscript in the model names is indicative of the mass of each model.

Model	M/M_\odot	R (km)	$\Delta r/R$ (%)	—	Model	M/M_\odot	R (km)	$\Delta r/R$ (%)
A+DH ₁₄	1.4	9.49	5.15		A+NV ₁₄	1.4	9.48	6.79
A+DH ₁₆	1.6	8.95	3.54		A+NV ₁₆	1.6	8.94	4.69
WFF3+DH ₁₄	1.4	10.82	6.45		WFF3+NV ₁₄	1.4	10.82	8.53
WFF3+DH ₁₆	1.6	10.61	4.98		WFF3+NV ₁₆	1.6	10.61	6.54
WFF3+DH ₁₈	1.8	10.03	3.54		WFF3+NV ₁₈	1.8	10.03	4.64
APR+DH ₁₄	1.4	12.10	7.72		APR+NV ₁₄	1.4	11.93	9.98
APR+DH ₁₆	1.6	12.09	6.23		APR+NV ₁₆	1.6	11.95	8.08
APR+DH ₁₈	1.8	12.03	5.05		APR+NV ₁₈	1.8	11.92	6.54
APR+DH ₂₀	2.0	11.91	4.05		APR+NV ₂₀	2.0	11.82	5.26
APR+DH ₂₂	2.2	11.65	3.15		APR+NV ₂₂	2.2	11.59	4.11
L+DH ₁₄	1.4	14.66	10.16		L+NV ₁₄	1.4	13.58	12.18
L+DH ₁₆	1.6	14.78	8.49		L+NV ₁₆	1.6	13.82	10.22
L+DH ₁₈	1.8	14.83	7.11		L+NV ₁₈	1.8	14.00	8.65
L+DH ₂₀	2.0	13.82	5.99		L+NV ₂₀	2.0	14.09	7.32
L+DH ₂₂	2.2	14.73	5.02		L+NV ₂₂	2.2	14.11	6.18
L+DH ₂₄	2.4	14.54	4.16		L+NV ₂₄	2.4	14.02	5.15
L+DH ₂₆	2.6	14.13	3.32		L+NV ₂₆	2.6	13.68	4.10

5 NUMERICAL RESULTS

5.1 Description of the EoS and equilibrium models

We have studied torsional modes for a variety of neutron star models using four different equations of state for the core, ranging from a very soft EoS (EoS A) (Pandharipande 1971) to a very stiff (EoS L) (Pandharipande & Smith 1975), with two intermediate ones, EoS WFF3 (Wiringa et al. 1988) and APR (Akmal et al. 1998). For each EoS we constructed a number of models, starting from a gravitational mass of $1.4M_\odot$ and reaching close to the maximum mass limit in increments of $0.2M_\odot$. In order to separately investigate the effect of the composition of the crust, we matched the various high-density EoS to two different proposed equations of state for the crust, one recent derived by Douchin & Haensel (2001) (DH) and, for reference, and older EoS by Negele & Vautherin (1973) (NV). Figure 2 displays the mass-radius relationship of nonrotating equilibrium models constructed with the various high-density EoS, in combination with our two choices for the crust EoS. The individual models for which we compute torsional modes are shown with symbols, while their detailed properties are listed in Table 1.

From Figure 2 it is evident that for the soft equations of state (A and WFF3) the choice of the crust EoS does not affect significantly the bulk properties of the star, while for the stiffest EoS L models with the same mass have considerably different radii. The reason for this is that the models constructed with the stiff EoS have central densities that are much closer to the density of the base of the crust than for soft EoS. The two crust EoS differ significantly both in the detailed composition, as well as in the density at the base of the crust, which is at $\rho \approx 2.4 \times 10^{14} \text{ gr/cm}^3$ for Negele & Vautherin (1973) and at $\rho \approx 1.28 \times 10^{14} \text{ gr/cm}^3$ for Douchin & Haensel (2001). For the stiff EoS these different properties of the crust have a considerable effect on the bulk properties.

For the two crust EoS the shear modulus μ can be computed using Equation (7). For the NV EoS a simple fitting formula was already derived by Duncan (1998)

$$\mu = 1.267 \times 10^{30} \text{ erg cm}^{-3} \rho_{14}^{4/5}, \quad (73)$$

which we also adopt here. For the DH EoS, we derive the following fitting (see also (Piro 2005))

$$\mu = 1.74 \times 10^{30} \text{ erg cm}^{-3} \rho_{14}^{4/3} \left(\frac{Z}{53} \right)^2 \left(\frac{616}{A} \right)^{4/3} \left(\frac{1 - X_n}{0.41} \right)^{4/3} \quad (74)$$

$$= 10^{30} \text{ erg cm}^{-3} (0.02123 + 0.37631 \rho_{14} + 3.13044 \rho_{14}^2 - 4.71841 \rho_{14}^3 + 2.46792 \rho_{14}^4) \quad (75)$$

where X_n is the fraction of nucleons in the neutron gas outside nuclei.

5.2 Torsional-mode frequencies in the non-magnetized limit

Even though the excitation of these modes and the SGR activity are likely related to the strong magnetic field, the torsional mode frequencies are not affected by the magnetic field for $B < 10^{15} \text{ G}$ (at least when the latter is confined to the crust). It is not clear whether magnetars have magnetic fields that only approach this value or that are even stronger. One should therefore first consider torsional mode frequencies in the non-magnetized limit.

In Table 2 we list the frequencies of the fundamental and torsional modes ℓt_0 for $\ell = 2$ to $\ell = 10$, for the equilibrium models discussed earlier and shown in Table 1. In addition to those models, we computed a few more i.e. L+DH₁₇, L+NV₁₉, and L+NV₂₅ in an attempt to fit the observed frequencies to given models. Among these models, the frequency of the fundamental $\ell = 2$ mode varies from 17 to 29 Hz i.e. depending on the stellar parameters it can vary by up to 30-50%. Limiting attention to models with $M = 1.4M_{\odot}$ only, the variation is from 21 to 29 Hz, which still significant. Therefore, strong constraints of the high-density EoS could be placed by observations of the fundamental $\ell = 2$ torsional mode in magnetars, especially if the mass is deduced by other means. On the other hand, the choice of the crust EoS does not seem to affect significantly the frequency of the fundamental torsional mode. The typical variation observed for equal mass models with different crust EoS is on the order of 1-5%. The same comments apply to the behavior of higher ℓ modes, which are nearly equally spaced for $\ell \geq 3$, such that a scaling law can be derived for each model.

The above picture is drastically altered when one considers the first overtone, ℓt_1 , for which the obtained frequencies are shown in Table 3. We observe that our numerical data are in agreement with the conclusion in Hansen & Cioffi (1980) that the frequencies are practically independent of the harmonic index ℓ . A second observation is that the variations in the frequencies due to different choices of both the high-density and crust EoS are significant. Notice that these observations apply for the higher overtones ℓf_n as well. The frequencies of the first overtones vary from 500-1200 Hz, while even for models with the same high-density EoS and same mass the frequency varies by up to 30% when changing the crust EoS. This behavior is quite useful given that there are suggestions for an observation in the spectrum of SGR 1802+14 of a torsional mode with $n = 1$ with a frequency of 626.5Hz (Watts & Strohmayer 2006) and at least one more at 1837 Hz. Comparing this to our results in Table 3 one could immediately exclude the soft and intermediate EoS A and WFF3, if the magnetic field is such that it does not affect the torsional mode frequencies. The $1.4M_{\odot}$ model of EoS APR with an NV description of the crust agrees with the observation, as does the $2.0M_{\odot}$ model with EoS L and NV for the crust. EoS L also seems to be compatible with the observation when combined with the DH crust EoS for a mass somewhat larger than $1.6M_{\odot}$. Finally, one can observe also that as the stellar mass increases the fundamental mode frequency decreases while the frequency of the 1st overtone increases. Note that this last observation also applies for the frequencies of the higher overtones as well (also see Table 4).

In the tables we have marked the frequencies which are close to the observed ones (within 2%) as bold for the source SGR 1806-20, underlined for the source SGR 1900+14 and italic for the source SGR 0526-66. One can observe that some of the stiff models fit quite well to the observational data i.e. model L+NV₂₅ (where ${}_{17}f_0 = 153$ Hz) for SGR 1900+14. Still, model A+DH₁₆ fits quite well with the observed frequencies of SGR 1900+14 and the $\ell = 11$ fundamental mode (not shown in the above tables) is exactly at 155 Hz. On the other hand, for SGR 1806-20 the models L+DH₁₇ (where ${}_{15}f_0 = 155$ Hz) or L+NV₂₀ (where ${}_{15}f_0 = 152$ Hz) are in good agreement with the observational data. According to our estimates, the observed frequencies of 18, 29, 92.5, 150, 626.5, and 1837 Hz would correspond to ${}_{2}f_0$, ${}_{3}f_0$, ${}_{9}f_0$, ${}_{15}f_0$, ℓf_1 , and ℓf_4 , respectively, although it is difficult to explain the observational data of 26 Hz because this data is very close to the other data of 29 Hz and it may be difficult to explain both frequencies by crustal torsional modes only. Additionally, model APR+NV₁₄ also agrees well with the observational data for SGR 1806-20. In the this non-magnetized limit, the currently available observational data appear to exclude softer EoS, such as EoS A and WFF3, if crustal torsional modes are invoked in interpreting the data.

5.3 Implications for crust thickness

As mentioned in the Introduction, one expects a simple relation between the thickness of the crust, $\Delta r/R$ and the ratio of the frequencies of the fundamental mode and higher harmonics, Equation (3). Using our numerical results, we can test the validity of the expected relation and attempt to infer the thickness of the crust from the observed frequencies in several SGRs. We construct the following empirical formula for the crust thickness

$$\frac{\Delta r}{R} \approx \ell \beta_n \frac{\ell f_0}{\ell f_n}. \quad (76)$$

where $\ell \beta_n$ are fitting coefficients. Using our numerical results presented in previous sections we find for the most interesting case of $\ell = 2$ and for $n = 0$ and $n = 1$ the fitted values ${}_{2}\beta_1 = 2.23 \pm 0.29$ for all models with a crust described by the NV EoS and ${}_{2}\beta_1 = 2.19 \pm 0.28$ for the corresponding models with a crust described by the DH EoS. These values are somewhat larger than the ones shown in the approximate relation (3), but this should be expected, since the Equation (3) was based on Newtonian dynamics and heuristic arguments.

Using the above empirical relation, important conclusions can be drawn for the stellar models listed in Table 1. The observed frequencies of SGR 1806-20 SGR, $\ell f_0 = 18$ Hz and $\ell f_1 = 626.5$ Hz suggest a crust ratio $\Delta r/R \approx 0.06$ which combined with the observed frequencies favors the model L+NV₂₂. Although, this conclusion is based on a single observation, it is still very important because it favors neutron star models with a very stiff equation of state, implying considerably larger masses than the typical ones. One should still keep in mind that there is an uncertainty regarding the observed frequency at 18Hz. If the actual frequency for the ℓf_0 mode is at 29Hz then the empirical formula (76) implies $\Delta r/R \approx 0.10$, which suggest stellar models with considerable smaller mass such as APR+NV₁₄ again, or ones with even smaller mass.

Table 2. Frequencies (in Hz) of the fundamental torsional modes in the non-magnetized limit (i.e. $n = 0$ and $B = 0$). Values in bold type, underline, and italic type are within 2% of observational data for SGR 1806-20, SGR 1900+14, and SGR 0526-66, respectively.

Model	$\ell = 2$	$\ell = 3$	$\ell = 4$	$\ell = 5$	$\ell = 6$	$\ell = 7$	$\ell = 8$	$\ell = 9$	$\ell = 10$
A+DH ₁₄	28.5	45.1	60.5	75.4	90.1	104.7	119.2	133.7	148.1
A+DH ₁₆	27.2	<u>43.0</u>	57.7	72.0	86.0	99.9	113.8	127.6	141.3
WFF3+DH ₁₄	26.3	41.6	55.9	69.7	<u>83.3</u>	96.8	110.2	123.5	136.8
WFF3+DH ₁₆	25.2	39.9	<u>53.5</u>	66.8	79.8	92.7	105.5	118.4	131.1
WFF3+DH ₁₈	24.3	38.4	51.5	64.3	76.8	89.3	101.6	114.0	126.2
APR+DH ₁₄	24.6	38.9	52.2	65.1	77.8	90.4	102.9	115.4	127.8
APR+DH ₁₆	23.4	37.0	49.6	61.9	73.9	85.9	97.8	109.6	121.5
APR+DH ₁₈	22.3	35.2	47.3	58.9	70.4	81.9	93.2	104.5	115.7
APR+DH ₂₀	21.3	33.6	45.1	56.3	67.3	78.1	89.0	99.7	110.5
APR+DH ₂₂	20.2	31.9	<u>42.8</u>	<u>53.4</u>	63.8	74.1	<u>84.4</u>	94.6	104.8
L+DH ₁₄	21.6	34.1	45.7	60.0	68.1	79.1	90.1	101.0	111.9
L+DH ₁₆	20.6	32.5	<u>43.7</u>	<u>54.5</u>	65.1	75.6	86.1	96.5	106.9
L+DH ₁₇	20.1	31.8	42.6	<u>53.2</u>	63.5	73.8	<u>84.0</u>	94.2	104.4
L+DH ₁₈	19.7	31.1	41.7	52.0	62.2	72.2	82.3	92.2	102.2
L+DH ₂₀	18.9	29.9	40.2	50.1	59.9	69.6	79.2	88.8	98.4
L+DH ₂₂	18.2	28.8	38.6	48.1	57.5	66.8	76.1	<u>85.3</u>	94.5
L+DH ₂₄	17.5	<u>27.7</u>	37.2	46.4	55.5	64.5	73.4	82.3	91.2
L+DH ₂₆	17.0	26.8	36.0	44.8	<u>53.6</u>	62.3	70.9	79.5	88.1
A+NV ₁₄	28.7	45.4	60.9	76.0	90.8	105.4	120.2	134.7	149.2
A+NV ₁₆	27.4	<u>43.3</u>	58.1	72.4	86.6	100.6	114.5	128.4	142.2
WFF3+NV ₁₄	26.7	42.2	56.6	70.6	<u>84.4</u>	98.1	111.6	125.2	138.6
WFF3+NV ₁₆	25.4	40.2	<u>53.9</u>	67.2	80.4	93.4	106.3	119.2	132.0
WFF3+NV ₁₈	24.4	38.6	51.7	64.5	77.1	89.6	102.0	114.4	126.7
APR+NV ₁₄	25.2	39.8	<u>53.4</u>	66.6	79.5	92.4	105.2	118.0	130.7
APR+NV ₁₆	23.8	37.6	50.5	63.0	75.3	87.5	99.6	111.7	123.7
APR+NV ₁₈	22.6	35.7	47.9	59.8	71.4	<u>83.0</u>	94.5	106.0	117.4
APR+NV ₂₀	21.4	33.9	45.5	56.7	67.8	78.8	89.7	100.5	111.4
APR+NV ₂₂	20.3	32.1	<u>43.1</u>	<u>53.8</u>	64.3	74.7	<u>85.0</u>	95.3	105.6
L+NV ₁₄	23.2	36.6	49.2	61.3	73.3	<u>85.1</u>	96.9	108.6	120.3
L+NV ₁₆	21.8	34.5	46.3	57.7	69.0	80.2	91.3	102.4	113.4
L+NV ₁₈	20.7	32.7	<u>43.9</u>	<u>54.7</u>	65.4	76.0	86.5	97.0	107.4
L+NV ₁₉	20.2	31.9	<u>42.8</u>	<u>53.3</u>	63.8	74.1	<u>84.3</u>	94.6	104.8
L+NV ₂₀	19.7	31.1	41.7	52.1	62.2	72.3	82.3	92.3	102.2
L+NV ₂₂	18.8	29.7	39.8	49.7	59.4	69.0	78.6	88.1	97.6
L+NV ₂₄	18.0	<u>28.4</u>	38.1	47.5	56.8	65.9	75.1	<u>84.2</u>	93.3
L+NV ₂₅	17.6	<u>27.8</u>	37.3	46.5	55.5	64.5	73.5	<u>82.4</u>	91.2
L+NV ₂₆	17.2	27.2	36.5	45.5	<u>54.4</u>	63.2	71.9	80.6	89.3

5.4 Effect of the magnetic field

We have already discussed earlier the possible effect of the magnetic field on the frequencies of the various torsional modes, when the magnetic field is confined to the crust. An approximate formula for the effect of the magnetic field based on Newtonian physics has been suggested by Duncan (1998), see also a detailed discussion by Messios et al. (2001). The formula suggests that the corrections in the frequency coming from the magnetic field scale as B^2 i.e.

$$\frac{\ell f_n}{\ell f_n^{(0)}} = \left[1 + \left(\frac{B}{B_\mu} \right)^2 \right]^{1/2} \quad (77)$$

where $\ell f_n^{(0)}$ is the frequency in the absence of any magnetic field and B_μ is a typical magnetic field strength at which magnetic field effects on torsional modes have become important, which we take here to be $B_\mu = 4 \times 10^{15}$ G. In the limit of $B \ll B_\mu$, this result agrees with earlier studies of the effect of the magnetic field on spheroidal modes derived by Carroll et al. (1986) and Unno et al. (1989), where the effect of the magnetic field has been shown to have the behavior

$$f \approx f^{(0)} + \ell \tilde{\alpha}_n B^2 \quad (78)$$

where $\ell \tilde{\alpha}_n$ is a coefficient depending on the parameters of the star (M , R and EoS) and it can be derived easily if the eigenfunctions of a specific mode are available. When one uses general relativity to calculate the frequencies of the torsional

Table 3. Frequencies (in Hz) of the first overtone of torsional modes in the non-magnetized limit (i.e. $n = 1$ and $B = 0$). Values in bold type are within about 2% of observational data for SGR 1806-20.

EoS	$\ell = 2$	$\ell = 3$	$\ell = 4$	$\ell = 5$	$\ell = 6$	$\ell = 7$	$\ell = 8$	$\ell = 9$	$\ell = 10$
A+DH ₁₄	1206.2	1206.8	1207.6	1208.6	1209.7	1211.1	1212.7	1214.5	1216.4
A+DH ₁₆	1531.3	1531.7	1532.3	1533.0	1533.9	1534.9	1536.0	1537.3	1538.7
WFF3+DH ₁₄	942.4	943.0	943.9	945.0	946.3	947.8	949.6	951.5	953.7
WFF3+DH ₁₆	1101.1	1101.6	1102.3	1103.2	1104.2	1105.4	1106.8	1108.3	1110.0
WFF3+DH ₁₈	1367.2	1367.6	1368.1	1368.7	1369.5	1370.4	1371.4	1372.5	1373.8
APR+DH ₁₄	761.3	762.0	762.9	764.1	765.5	767.1	769.0	771.1	773.4
APR+DH ₁₆	860.2	860.8	861.5	862.5	863.6	864.9	866.4	868.1	869.9
APR+DH ₁₈	965.6	966.0	966.6	967.4	968.3	969.4	970.6	972.0	973.5
APR+DH ₂₀	1083.3	1083.6	1084.1	1084.8	1085.5	1086.4	1087.3	1088.4	1089.7
APR+DH ₂₂	1238.0	1238.3	1238.7	1239.2	1239.8	1240.5	1241.2	1242.1	1243.1
L+DH ₁₄	530.2	531.0	532.0	533.3	534.8	536.6	538.7	540.9	543.4
L+DH ₁₆	586.4	587.0	587.9	588.9	590.2	591.7	593.4	595.2	597.3
L+DH ₁₇	617.0	617.6	618.4	619.4	620.5	621.9	623.4	625.1	627.0
L+DH ₁₈	648.1	648.6	649.3	650.2	651.3	652.5	653.9	655.5	657.2
L+DH ₂₀	712.5	712.9	713.5	714.2	715.1	716.2	717.3	718.7	720.1
L+DH ₂₂	788.1	788.5	789.0	789.6	790.3	791.2	792.2	793.3	794.5
L+DH ₂₄	874.2	874.5	875.0	875.5	876.1	876.8	877.7	878.6	879.6
L+DH ₂₆	995.1	995.4	995.7	996.2	996.7	997.3	997.9	998.7	999.5
A+NV ₁₄	951.0	951.7	952.8	954.0	955.6	957.3	959.4	961.6	964.2
A+NV ₁₆	1190.8	1191.4	1192.1	1193.1	1194.2	1195.5	1197.0	1198.6	1200.5
WFF3+NV ₁₄	740.8	741.6	742.7	744.1	745.8	747.8	750.0	752.5	755.3
WFF3+NV ₁₆	865.8	866.5	867.4	868.5	869.8	871.3	873.1	875.0	877.2
WFF3+NV ₁₈	1069.8	1070.3	1071.0	1071.8	1072.8	1073.9	1075.2	1076.7	1078.4
APR+NV ₁₄	616.5	617.3	618.5	620.0	621.8	623.9	626.3	628.9	631.8
APR+NV ₁₆	688.5	689.2	690.2	691.4	692.8	694.5	696.4	698.5	700.9
APR+NV ₁₈	769.4	770.0	770.7	771.7	772.9	774.2	775.8	777.5	779.5
APR+NV ₂₀	858.3	858.7	859.4	860.2	861.1	862.2	863.5	864.9	866.4
APR+NV ₂₂	974.4	974.7	975.2	975.9	976.6	977.5	978.5	979.6	980.9
L+NV ₁₄	483.6	484.6	485.9	487.5	489.4	491.6	494.1	496.9	500.1
L+NV ₁₆	524.6	525.4	526.4	527.7	529.3	531.1	533.2	535.6	538.1
L+NV ₁₈	567.7	568.3	569.2	570.3	571.6	573.2	574.9	576.9	579.0
L+NV ₁₉	589.7	590.3	591.1	592.1	593.4	594.8	596.4	598.2	600.1
L+NV ₂₀	614.9	615.4	616.2	617.1	618.2	619.5	621.0	622.6	624.4
L+NV ₂₂	667.1	667.5	668.2	668.9	669.9	670.9	672.2	673.6	675.1
L+NV ₂₄	729.1	729.5	730.0	730.7	731.4	732.3	733.4	735.6	735.9
L+NV ₂₅	769.8	770.2	770.7	771.3	772.0	772.8	773.8	774.8	776.0
L+NV ₂₆	824.1	824.4	824.8	825.3	826.0	826.7	827.6	828.5	829.6

modes the relativistic effects such as the relativistic form of the sound speed, the redshift corrections and the EoS affect the weighting factor $\ell\alpha_n$ of equation (78) and have to be taken properly into account.

In our numerical calculations of the torsional modes of magnetized neutron stars for the various EoS mentioned earlier we derived lists of frequencies for every model, for magnetic field strengths up to $B = 10^{17}$ G. By numerical fitting we have thus found the coefficients $\ell\alpha_n$ of the following empirical formula

$$\frac{\ell f_n}{\ell f_n^{(0)}} \approx \left[1 + \ell\alpha_n \left(\frac{B}{B_\mu} \right)^2 \right]^{1/2}. \quad (79)$$

The coefficients $\ell\alpha_n$ are listed in Table 5 and the way that the various EoS (both for the core and the crust) affect the torsional frequencies becomes apparent. In general, it seems that models constructed with the DH equation of state are affected significantly more by the magnetic field than models following the NV EoS, for all harmonics. As a result, the large differences in the torsional mode frequencies between models constructed with the stiffest EoS L but with different crust EoS are diminished by magnetic field effects around $B = 4 \times 10^{15}$ G and reversed for larger values of B .

When the magnetic field strength is equal to $B = B_\mu = 4 \times 10^{15}$ G the frequencies have increased by up to 35% for the fundamental torsional mode (independently of the value of ℓ) and up to 100% for the first overtone. The results suggest that for magnetic field strengths exceeding roughly 10^{15} G the shift in the frequencies is significant and should be taken into account in any attempt to fit the observational data with specific stellar models.

Table 4. Frequencies (in Hz) of the overtone of torsional modes for $\ell = 2$ and $n = 2, 3$, and 4 in the non-magnetized limit (i.e. $B = 0$). Values in bold type are within about 2% of observational data for SGR 1806-20.

EoS	$n = 2$	$n = 3$	$n = 4$
A+DH ₁₄	2011.4	2774.8	3476.4
A+DH ₁₆	2552.6	3521.8	4412.2
WFF3+DH ₁₄	1572.0	2164.7	2708.7
WFF3+DH ₁₆	1835.8	2530.7	3167.6
WFF3+DH ₁₈	2278.2	3142.1	3933.3
APR+DH ₁₄	1270.0	1747.9	2186.8
APR+DH ₁₆	1434.7	1976.0	2472.5
APR+DH ₁₈	1610.0	2218.8	2776.6
APR+DH ₂₀	1805.4	2489.4	3115.8
APR+DH ₂₂	2062.9	2844.2	3559.7
L+DH ₁₄	885.1	1217.6	1525.1
L+DH ₁₆	978.6	1347.9	1688.6
L+DH ₁₇	1029.7	1418.7	1777.3
L+DH ₁₈	1081.5	1490.4	1867.3
L+DH ₂₀	1188.4	1639.2	2054.1
L+DH ₂₂	1314.4	1813.3	2272.4
L+DH ₂₄	1457.6	2011.5	2521.1
L+DH ₂₆	1658.5	2289.4	2869.5
A+NV ₁₄	1687.9	2390.3	2905.7
A+NV ₁₆	2113.5	2997.8	3675.8
WFF3+NV ₁₄	1315.1	1860.7	2250.9
WFF3+NV ₁₆	1536.7	2176.5	2647.9
WFF3+NV ₁₈	1898.3	2691.5	3295.1
APR+NV ₁₄	1094.5	1547.3	1864.0
APR+NV ₁₆	1222.4	1730.5	2098.8
APR+NV ₁₈	1365.6	1934.5	2355.3
APR+NV ₂₀	1523.2	2159.5	2641.2
APR+NV ₂₂	1728.8	2452.0	3008.3
L+NV ₁₄	858.9	1212.6	1453.1
L+NV ₁₆	931.5	1316.9	1586.8
L+NV ₁₈	1007.9	1426.4	1727.1
L+NV ₁₉	1047.1	1482.6	1799.9
L+NV ₂₀	1091.6	1546.0	1879.5
L+NV ₂₂	1184.1	1678.3	2048.6
L+NV ₂₄	1294.1	1835.3	2248.6
L+NV ₂₅	1366.2	1937.6	2375.4
L+NV ₂₆	1462.3	2074.3	2546.7

In Figures 3 and 4 we show some examples of the effect of the magnetic field on the torsional mode frequencies. Notice that for $B < B_\mu$ the effect of the magnetic field on the frequencies follows a quadratic increase, in agreement with the approximate relation (78). On the other hand, when $B > B_\mu$ the modes change character and become dominated by the magnetic field, while the frequencies tend to become less sensitive to the stellar parameters. In this regime, additional effects, such as the coupling to global magnetosonic waves and to higher-order harmonics should be taken into account.

6 SUMMARY AND DISCUSSION

We have derived the formalism for computing torsional oscillations of relativistic stars endowed with a strong dipole magnetic field, confined to the crust. Our equations are valid in the Cowling approximation (no spacetime perturbations) and we have neglected the effect of the magnetic field on the equilibrium configuration and on the coupling of torsional modes to $\ell \pm 2$ terms and to global magnetosonic modes. Under these approximations, our formalism allows us to obtain an estimate of the magnetic field effects on torsional modes, up to moderate values of the magnetic field strength (up to a few times $B_\mu = 4 \times 10^{15}$ G). These moderate values of the magnetic field strength are appropriate for models of magnetars, for which there is strong evidence that they are at the heart of the SGR phenomenon.

We have done a systematic search of parameter space by computing torsional mode frequencies for various values of the harmonic index ℓ and for various overtones, using an extended sample of models of compact stars. These models vary in mass, high-density equation of state and crust model, uniformly covering the allowed mass vs. radius parameter space. Our

Table 5. The values for the fitting factors $\ell\alpha_n$ of equation (79). The fitting factors have been calculated for magnetic field strength up to 10^{17} G.

Model	$2\alpha_0$	$2\alpha_1$	$5\alpha_0$	$5\alpha_1$	$8\alpha_0$	$8\alpha_1$
A+DH ₁₄	0.38	1.44	0.67	1.63	0.70	1.65
A+DH ₁₆	0.39	1.34	0.70	1.52	0.73	1.55
WFF3+DH ₁₄	0.45	1.55	0.70	1.75	0.72	1.77
WFF3+DH ₁₆	0.42	1.43	0.68	1.62	0.71	1.64
APR+DH ₁₄	0.54	1.63	0.71	1.84	0.72	1.87
APR+DH ₁₆	0.50	1.53	0.70	1.73	0.72	1.75
APR+DH ₁₈	0.48	1.44	0.70	1.63	0.72	1.66
APR+DH ₂₀	0.48	1.37	0.70	1.55	0.72	1.57
APR+DH ₂₂	0.47	1.32	0.72	1.49	0.75	1.51
L+DH ₁₄	0.80	1.83	0.77	2.06	0.75	2.09
L+DH ₁₆	0.73	1.68	0.73	1.90	0.73	1.93
L+DH ₁₈	0.67	1.59	0.72	1.80	0.72	1.83
L+DH ₂₀	0.63	1.50	0.71	1.70	0.71	1.73
L+DH ₂₂	0.60	1.44	0.71	1.64	0.72	1.66
L+DH ₂₄	0.57	1.38	0.71	1.56	0.72	1.59
L+DH ₂₆	0.55	1.32	0.72	1.50	0.74	1.53
<hr/>						
A+NV ₁₄	0.26	0.56	0.32	0.63	0.33	0.64
A+NV ₁₆	0.24	0.50	0.32	0.57	0.33	0.58
WFF3+NV ₁₄	0.34	0.60	0.33	0.68	0.33	0.69
WFF3+NV ₁₆	0.30	0.55	0.33	0.62	0.33	0.63
APR+NV ₁₄	0.42	0.63	0.35	0.72	0.33	0.73
APR+NV ₁₆	0.38	0.58	0.34	0.66	0.33	0.67
APR+NV ₁₈	0.35	0.55	0.33	0.62	0.33	0.63
APR+NV ₂₀	0.32	0.52	0.33	0.59	0.33	0.60
APR+NV ₂₂	0.30	0.49	0.34	0.56	0.34	0.57
L+NV ₁₄	0.55	0.69	0.37	0.78	0.34	0.79
L+NV ₁₆	0.51	0.64	0.36	0.73	0.33	0.73
L+NV ₁₈	0.47	0.60	0.35	0.68	0.33	0.69
L+NV ₂₀	0.44	0.57	0.34	0.64	0.33	0.65
L+NV ₂₂	0.41	0.54	0.34	0.61	0.33	0.62
L+NV ₂₄	0.39	0.51	0.34	0.58	0.33	0.59
L+NV ₂₅	0.38	0.50	0.34	0.57	0.34	0.58
L+NV ₂₆	0.36	0.49	0.35	0.56	0.34	0.57

numerical results have shown that torsional mode frequencies are sensitive to the crust model if the high-density equation of state is very stiff (such as EoS L). In addition, torsional mode frequencies are drastically affected by a dipole magnetic field, if the latter has a strength exceeding roughly 10^{15} G. The effect of the magnetic field is surprisingly sensitive to the adopted crust model. Using our extended numerical results we have derived empirical relations for the effect of the magnetic field on torsional modes as well as for the crust thickness. We compare our numerical results to observed frequencies in SGRs and find that certain high-density EoS and mass values are favored over others in the non-magnetized limit. On the other hand, if the magnetic field is strong, then its effect has to be taken into account in attempts to formulate a theory of asteroseismology for magnetars. This topic, as well as the inclusion of global magnetosonic modes will be discussed in a separate publication (Sotani et al. 2006).

ACKNOWLEDGMENTS

We are grateful to Nils Andersson, Demetrios Papadopoulos, Adamantios Stavridis and Miltos Vavoulidis for useful discussions. This work was supported by the Marie-Curie grant MIF1-CT-2005-021979 and the Pythagoras II program of GSRT.

REFERENCES

- Akmal A., Pandharipande V.R., Ravenhall D.G., 1998, Phys. Rev. C 58, 1804
- Barat et al., 1983, A&A, 126, 400
- Bocquet M., Bonazzola S., Gourgoulhon E., Novak J., 1995, A&A, 301, 757
- Bonazzola S., Gourgoulhon E., Salgado M., Marck J.A., 1993, A&A, 278, 421

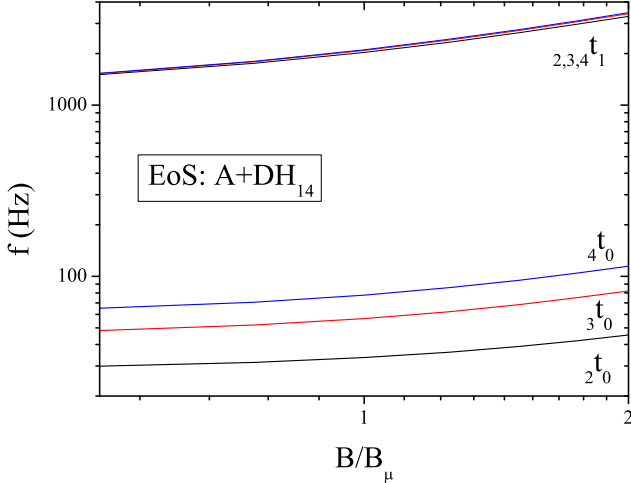


Figure 3. The frequencies of the fundamental $n = 0$ and the first overtone for $\ell = 2, 3$ and 4 torsional modes as functions of the normalized magnetic field (B/B_μ). The neutron star mass is $1.4M_\odot$ and we show results for EoS A+DH.

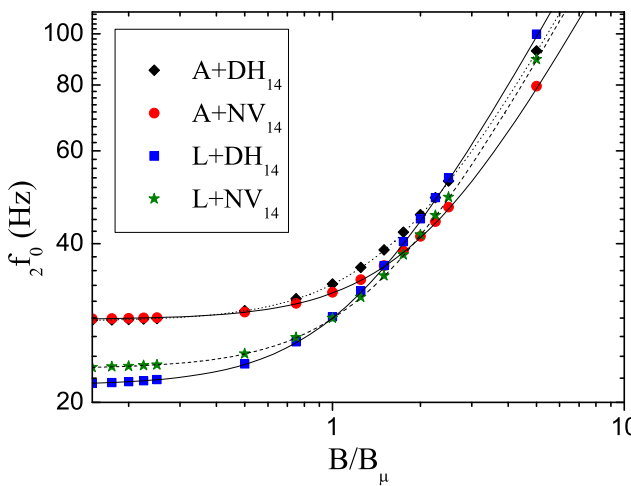


Figure 4. The frequencies of the fundamental $n = 0$ and $\ell = 2$ torsional mode as functions of the normalized magnetic field (B/B_μ). The neutron star masses are $1.4M_\odot$ and we show only results for four EoS i.e. A+DH, A+NV, L+DH and L+NV. The lines correspond to fits according to the empirical formula, Eq. (79), with coefficient values from Table 5. As seen here, our empirical formula, Eq. (79), agrees very well with the numerical results. We stress that these results were obtained in the approximation of neglecting magnetic-field-induced deformations of the background star and couplings to $\ell \pm 2$ terms.

Braithwaite J., Spruit H.C., A&A, 450, 1097

Carroll B.W., Zweibel E.G., Hansen C., McDermott P.N., Savedoff M.P., Thomas J.H., Van Horn H.M., 1986, ApJ, 305, 767

Carter B., Quintana H., 1973, Proc. R. Soc. Lond., A331, 57

Douchin F., Haensel P., 2001, A& A, 380, 151

Duncan R.C., 1998, ApJ, 1998, 498, L45

Duncan R.C., Thompson C., 1992, ApJ, 392, L9

Glampedakis K., Samuelson L., Andersson N., 2006, astro-ph/0605461

Hansen C., Cioffi D.F., 1980, ApJ, 238, 740

Hurley K. et al., 1999, Nature, 397, 41
 Israel G. et al., 2005, ApJ, 628, L53
 Konno K., Obata T., Kojima Y., 1999, A&A, 352, 211
 Lee, U., 2006, astro-ph/0610182
 Leins M., 1994, PhD Thesis, University of Tübingen
 Mazets E.P. et al., 1979, Nature 282, 587
 McDermott P.N., Van Horn H.M., Hansen C.J., 1988, ApJ, 325, 725
 Messios N., Papadopoulos D.B., Stergioulas N., 2001, MNRAS, 328, 1161 .
 Negele J.W., Vautherin D., 1973, Nucl. Phys., A207, 298
 Palmer D.M. et al., 2005, Nature, 434, 1107
 Pandharipande V.R., 1971, Nucl. Phys. A, 178, 123
 Pandharipande V.R., Smith R.A., 1975, Phys. Lett. 59B, 15
 Piro A.L., 2005, ApJ, 634, L153
 Samuelsson L., Andersson N., astro-ph/0609265
 Schumaker B.L., Thorne K.S., 1983, MNRAS, 203, 457
 Strohmayer T.E., 1991, ApJ, 372, 591
 Sotani H., Kokkotas, K.D., Stergioulas, N., Vavoulidis, M., preprint (astro-ph/0611666)
 Strohmayer T.E., et al., 1991, ApJ, 375, 679
 Strohmayer T.E., Watts A.L., 2005, ApJ, 632, L111
 Strohmayer T.E., Watts A.L., astro-ph/0608463 (accepted in ApJ)
 Terasawa T., et al., 2005, Nature 434, 1110
 Unno W., Osaki Y., Ando H., Saio H., Shibahashi H., 1989, Nonradial Oscillations of Stars, University of Tokyo Press
 Wasserman I., Shapiro S.L., 1983, ApJ, 265, 1036
 Watts A.L., Strohmayer T.E., 2006, ApJ, 637, L117
 Wiringa R.B., Fiks V., Farrocini A., 1988, Phys. Rev. C 38, 1010

APPENDIX A: MONOPOLE MAGNETIC FIELD

If the magnetic field is assumed to be axisymmetric, Maxwell's equations (13) become

$$H_{,r}^r + H_{,\theta}^{\theta} + \left(\Lambda' + \frac{2}{r} \right) H^r + \cot \theta H^{\theta} = 0. \quad (\text{A1})$$

As a toy model, we consider a monopolar magnetic field in the crust

$$H^r = H^r(r) \neq 0, \quad (\text{A2})$$

$$H^{\theta} = 0. \quad (\text{A3})$$

For this case, the solution of Maxwell's equation (A1) we is (Messios et al. 2001)

$$H^r = \frac{1}{r^2} e^{-\Lambda} C, \quad (\text{A4})$$

where C is some constant. For this case the perturbation equation (52) is rewritten as

$$\begin{aligned} -(\epsilon + p + H^r H_r) \omega^2 e^{-2\Phi+2\Lambda} \mathcal{Y} &= (\mu + H^r H_r) \mathcal{Y}'' \\ &+ \left[\left(\frac{4}{r} + \Phi' - \Lambda' \right) \mu + \mu' + (\Phi' - \Lambda') H^r H_r \right] \mathcal{Y}' - \frac{(\ell+2)(\ell-1)}{r^2} \mu e^{2\Lambda} \mathcal{Y} \end{aligned} \quad (\text{A5})$$

If we introduce the new variables, such as

$$\mathcal{Y}_1 \equiv \mathcal{Y}, \quad (\text{A6})$$

$$\mathcal{Y}_2 \equiv (\mu + H^r H_r) e^{\Phi-\Lambda} \mathcal{Y}_1', \quad (\text{A7})$$

then equations (A5) reduce

$$\mathcal{Y}_1' = \frac{1}{\mu + H^r H_r} e^{-\Phi+\Lambda} \mathcal{Y}_2, \quad (\text{A8})$$

$$\mathcal{Y}_2' = \left[\frac{(\ell+2)(\ell-1)}{r^2} \mu e^{2\Phi} - (\epsilon + p + H^r H_r) \omega^2 \right] e^{-\Phi+\Lambda} \mathcal{Y}_1 - \frac{4}{r} \mathcal{Y}_2 \quad (\text{A9})$$

In Figure A1 we show the fundamental and first overtone frequencies for neutron star models with mass $1.4M_{\odot}$. It is apparent that in the case of a monopole magnetic field the frequencies (especially of the fundamental mode) will be marginally

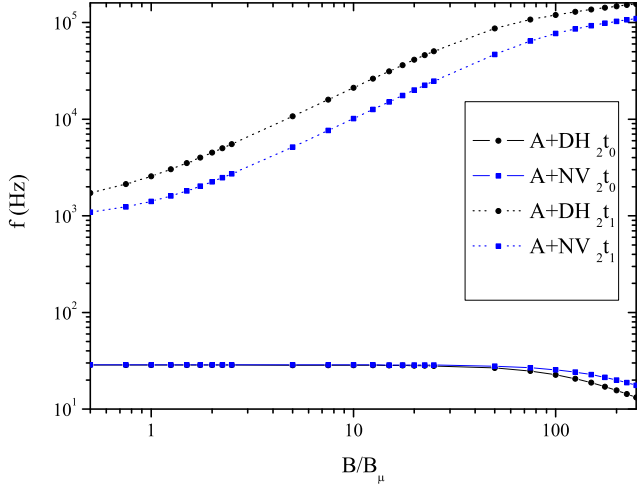


Figure A1. The frequencies of the $2t_0$ and $2t_1$ torsional modes as functions of the normalized magnetic field (B/B_μ) for EoS A+DH and A+NV are shown. The magnetic field has monopole geometry while the neutron stars have masses $1.4M_\odot$.

affected by the magnetic field and only for strengths on the order of 10^{17} G its influence becomes significant. This is in qualitative agreement with the conclusions in Messios et al. (2001). In addition, we confirm the finding in Messios et al. (2001) that the frequency of the fundamental mode decreases for a monopole magnetic field, as is apparent in Figure A1.